Acta Crystallographica Section F
Structural Biology and Crystallization Communications
ISSN 1744-3091

Crystallization and X-ray data analysis of the 10 kDa C-terminal lid subdomain from *Caenorhabditis elegans* Hsp70

Liam Worrall and Malcolm D. Walkinshaw*

School of Biological Sciences, University of Edinburgh, The King's Buildings, Mayfield Road, Edinburgh EH9 3JR, Scotland

Correspondence e-mail: m.walkinshaw@ed.ac.uk

Received 20 June 2006
Accepted 14 August 2006

Hsp70 is an important molecular chaperone involved in the regulation of protein folding. Crystals of the C-terminal 10 kDa helical lid domain (residues 542–640) from a *Caenorhabditis elegans* Hsp70 homologue have been produced that diffract X-rays to ~3.4 Å. Crystals belong to space group $I2_12_12_1$, with unit-cell parameters $a = b = 197$, $c = 200$ Å. The Matthews coefficient, self-rotation function and Patterson map indicate 24 monomers in the asymmetric unit, showing non-crystallographic 432 symmetry. Molecular-replacement studies using the corresponding domain from rat, the only eukaryotic homologue with a known structure, failed and a mercury derivative was obtained. Preliminary MAD phasing using *SHELXD* and *SHARP* for location and refinement of the heavy-atom substructure and *SOLOMON* for density modification produced interpretable maps with a clear protein–solvent boundary. Further density-modification, model-building and refinement are currently under way.

1. Introduction

Hsp70 is an essential molecular chaperone involved in numerous protein-folding processes. It belongs to a family of ubiquitously expressed proteins that exist in virtually all living organisms (Wegele *et al.*, 2004). Hsp70 consists of two domains: a 40 kDa N-terminal nucleotide-binding domain (NBD), which both binds and hydrolyses ATP, and a 30 kDa C-terminal substrate-binding domain (SBD) (Chappell *et al.*, 1987). The SBD can be further divided into an 18 kDa β-sandwich subdomain, which forms a hydrophobic peptide-binding groove capable of binding exposed hydrophobic patches on proteins, and a 10 kDa helical bundle subdomain that forms a lid over the peptide-binding groove (Zhu *et al.*, 1996). Substrate binding and release is an allosteric process, with cycles of ATP binding and hydrolysis in the NBD controlling the accessibility of the hydrophobic binding groove of the SBD (Flynn *et al.*, 1989; Takeda & McKay, 1996; Mayer *et al.*, 2000). The exact mechanism of this regulation is not well understood. Proposals involve either a hinge-mediated movement of the lid subdomain or the melting of some of the helical segments in the lid (Mayer *et al.*, 2000; Jiang *et al.*, 2005; Fernandez-Saiz *et al.*, 2006; Rist *et al.*, 2006).

Structures are available for both the NBD (Flaherty *et al.*, 1990) and SBD (Zhu *et al.*, 1996; Wang *et al.*, 1998; Morshauser *et al.*, 1999; Pellecchia *et al.*, 2000). The only structure incorporating both domains is the recently published bovine structure (residues 1–554), which lacks most of the C-terminal lid (Jiang *et al.*, 2005). This structure reveals interdomain interactions that are implicated in the allosteric regulation. The only eukaryotic structure solved for the 10 kDa C-terminal lid domain is that from rat (Chou *et al.*, 2003), which has an antiparallel coiled-coil mediated dimer. This is in contrast to the monomeric three-helical bundle observed in the *Escherichia coli* homologue DnaK (Zhu *et al.*, 1996), which shares approximately 17% sequence identity (Fig. 1). Since it is the lid domain that restricts access to the peptide-binding groove, structural knowledge of this domain should increase understanding of the process of client binding and release.

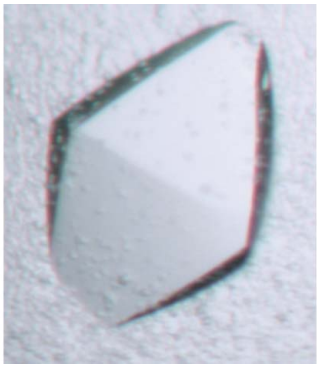

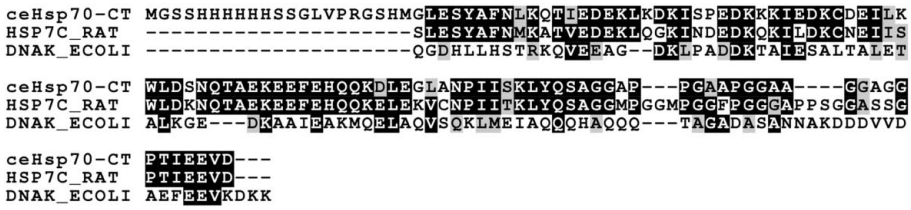

Figure 1
Sequence alignment of the recombinant *C. elegans* C-terminal Hsp70 sequence used in this study with Hsp70 homologues of known structure from rat (∼69% sequence identity; Chou *et al.*, 2003) and *E. coli* (∼17% sequence identity; Zhu *et al.*, 1996). Identical residues shared by two sequences are shaded in black and similar residues shaded in grey. The alignment was produced with *MUSCLE* (Edgar, 2004) and the figure was produced with *BOXSHADE*. Sequence identity calculated as number of aligned residues/alignment length.

Here, we describe the expression, purification, crystallization, X-ray data analysis and preliminary heavy-atom phasing of the 10 kDa lid subdomain from *Caenorhabditis elegans* Hsp70.

2. Experimental procedures

2.1. Cloning and expression

The cDNA fragment corresponding to residues 542–640 of the *C. elegans* Hsp70 homologue hsp-1 (gene F26D10.3; now designated ceHsp70-CT) was generated by polymerase chain reaction (PCR) using *C. elegans* mixed-stage N2 cDNA as a template. The sequence was amplified with the TaqPlus precision PCR system (Stratagene) using forward (GCGG**CATATG**GGACTCGAGTCATACGCCTTC) and reverse primers (GCGG**GCGGCCGC**TTAGTCGACCTCCTC-TTAGTCGACCTCCTCGATC). The resulting PCR product was cloned into a pCR2.1 TOPO vector (Invitrogen) and digested with *Nde*I and *Not*I (New England Biolabs; cutting sites are shown in bold). The digested insert was ligated into a similarly digested pET-28a vector (Novagen) downstream of the 6×His coding region. The correct sequence was verified by sequencing.

Recombinant ceHsp70-CT was expressed in Rosetta2(DE3) *E. coli* (Novagen) in LB liquid medium containing kanamycin (25 µg ml^{-1}) and chloramphenicol (30 µg ml^{-1}). Cultures were grown with shaking at 310 K until the A_{600} was ∼0.6 and expression was induced by addition of 1 m*M* isopropyl β-D-thiogalactopyranoside (IPTG). Expression was continued for 4 h and cells were harvested by centrifugation (3000*g* for 15 min).

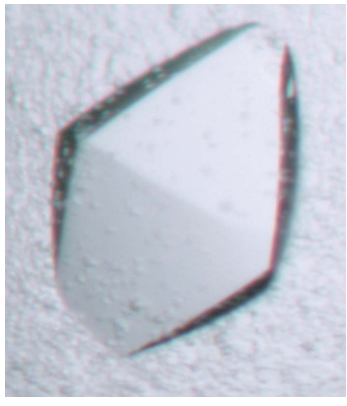

Figure 2
Example of ceHsp70-CT crystal grown in 62% saturated ammonium sulfate buffered by sodium citrate pH 6.0. Maximum dimension is ∼0.6 mm.

2.2. Purification

Cell pellets were resuspended at 10%(*w*/*v*) in ice-cold lysis buffer (buffer *A*; 50 m*M* sodium phosphate pH 8.0, 100 m*M* NaCl, 0.1 m*M* benzamidine, 0.1 m*M* PMSF) plus excess protease-inhibitor cocktail (Roche) and sonicated on ice for 6 × 30 s bursts with 30 s cooling in between. The cell lysate was subjected to centrifugation at 30 000*g* for 1 h at 277 K. The supernatant was filtered through a 0.2 µm filter and applied onto a 10 ml Ni–NTA Superflow (Qiagen) column pre-equilibrated in wash buffer (buffer *B*; 50 m*M* sodium phosphate pH 8.0, 100 m*M* NaCl, 10 m*M* imidazole). Proteins were eluted with a stepped imidazole gradient (buffer *C*; 50 m*M* sodium phosphate pH 8.0, 100 m*M* NaCl, 250 m*M* imidazole). Weakly binding protein was washed off with 10% buffer *C* and 6×His-tagged ceHsp70-CT eluted with 30% buffer *C*. Fractions containing recombinant protein were pooled, concentrated to ≤1 ml, filtered through a 0.2 µm filter and loaded onto a Sephacryl-200 HR (Pharmacia) gel-filtration column ($V_t \simeq 120$ ml; 1.6 × 60 cm) equilibrated in buffer *D* (25 m*M* HEPES pH 7.5, 50 m*M* KCl, 1 m*M* DTT). Recombinant ceHsp70-CT eluted from the Sephacryl-200 column as a single peak and was more than 95% pure as judged by SDS–PAGE. Protein was stored on ice at 277 K in buffer *D*.

2.3. Crystallization and preparation of a heavy-atom derivative

Crystals of the 10 kDa subdomain, including the recombinant His tag, were grown by the hanging-drop vapour-diffusion method from a 12 mg ml^{-1} protein solution in buffer *D* at 291 K. Initial conditions were identified with an ammonium sulfate grid screen. The best crystals were obtained using a well solution of 62% saturated ammonium sulfate buffered by 100 m*M* sodium citrate pH 6.0 with a 2 µl drop consisting of a 1:1 ratio of protein and well solution. Crystals appeared within 24 h and grew to dimensions of 0.6 × 0.4 × 0.4 mm over three weeks (Fig. 2). Conditions were comparable to those published for the rat homologue (Chou *et al.*, 2001, 2003). A mercury derivative was obtained by soaking native crystals for 30 min in well solution containing 5 m*M* mercuric chloride followed by back-soaking for 30 s in well solution. All crystals were flash-cooled in liquid nitrogen prior to data collection, either directly from mother liquor or with prior soaking in cryoprotectant containing 70% saturated ammonium sulfate and 10% glycerol.

2.4. Data collection and processing

Data were collected at station 10.1, SRS, Daresbury, UK for the native data set I and station BM14, ESRF, Grenoble, France for the native data set II and the mercury-derivative crystal. All data were collected at 100 K. MAD data were collected from a single derivative crystal at two wavelengths, corresponding to the mercury L_{III} peak (1.005 Å) and the L_{III}-edge inflection point (1.009 Å). All data were

Table 1
Reflection data statistics for data processed in space groups $I4_122$ and $I2_12_12_1$.

Values in parentheses are for the highest resolution bin.

Data set	Native I		Native II		Hg L_{III} peak		Hg L_{III} inflection	
Cryoprotectant	Mother liquor		70% ammonium sulfate, 10% glycerol		Mother liquor		Mother liquor	
Beamline	SRS, 10.1		ESRF, BM14		ESRF, BM14		ESRF, BM14	
φ rotation (°)	120, 1° step		180, 1.5° step		100, 1° step		100, 1° step	
Temperature (K)	100		100		100		100	
Wavelength (Å)	1.005		0.978		1.005		1.009	
Space group	$I4_122$	$I2_12_12_1$	$I4_122$	$I2_12_12_1$	$I4_122$	$I2_12_12_1$	$I4_122$	$I2_12_12_1$
Unit-cell parameters (Å)								
a (Å)	196.9	196.8	194.7	194.6	195.1	195.1	195.5	195.5
b (Å)	196.9	196.9	194.7	195	195.1	195.2	195.5	195.6
c (Å)	200.6	200.6	200.8	200.8	202.8	202.8	203.5	203.4
Resolution range (Å)	45–3.95 (4.16–3.95)	45–3.95 (4.16–3.95)	35–3.4 (3.58–3.4)	35–3.4 (3.58–3.4)	42–3.95 (4.16–3.95)	42–3.95 (4.16–3.95)	42–4.1 (4.32–4.1)	42–4.1 (4.32–4.1)
No. of observations	131543 (16631)	131659 (16730)	399719 (58219)	388320 (56298)	142589 (21135)	142701 (21069)	128025 (18741)	128245 (18752)
No. of unique reflections	17565 (2516)	32857 (4723)	26797 (3841)	52659 (7591)	16504 (2420)	31088 (4612)	14849 (2151)	27844 (4089)
Completeness	99.8 (99.8)	95.3 (95.5)	99.9 (100)	99.9 (99.9)	95.0 (96.1)	91.5 (93.2)	94.8 (95.8)	90.9 (92.5)
Anomalous completeness					94.6 (95.6)	86.1 (87.5)	94.2 (95.2)	85.0 (86.3)
Multiplicity	7.8	4.0 (3.5)	14.9 (15.2)	7.4 (7.4)	8.6 (8.7)	4.6 (4.5)	8.6 (8.7)	4.6 (4.6)
Anomalous multiplicity					4.6 (4.5)	2.5 (2.4)	4.6 (4.5)	2.5 (2.5)
R_{sym}† (%)	12.8 (88.8)	11.3 (76.8)	29.1 (116.3)	15.5 (111.1)	11.0 (73.9)	10.1 (70.8)	10.4 (102.9)	12.0 (105.4)
$R_{p.i.m.}$‡ (%)	5.0 (35.5)	6.0 (44.3)	7.4 (25.4)	6.1 (43.5)	4.7 (27.3)	6.2 (37.4)	4.1 (37.5)	6.6 (63.5)
$I/\sigma(I)$	14.2 (3.0)	10.5 (2.4)	10.1 (1.6)	10.1 (1.6)	13.7 (2.5)	10.0 (1.9)	13.9 (2.1)	9.9 (1.4)

† $R_{sym} = \sum_{hkl}\sum_i |I_i(hkl) - \langle I(hkl)\rangle| / \sum_{hkl}\sum_i |I_i(hkl)|$, ‡ $R_{p.i.m.} = \sum_{hkl}[1/(N-1)]^{1/2}\sum_i |I_i(hkl) - \langle I(hkl)\rangle| / \sum_{hkl}\sum_i |I_i(hkl)|$ (Diederichs & Karplus, 1997), where $I_i(hkl)$ and $\langle I(hkl)\rangle$ are the observed individual and mean intensities of a reflection with indices hkl, respectively, $\sum_i$ is the sum over the individual measurements of a reflection with indices hkl, $\sum_{hkl}$ is the sum over all reflections and N is the redundancy. A mean $I/\sigma(I)$ of between 1.5 and 2 was used to define the lower resolution limit unless ice diffraction interfered with processing.

indexed and integrated using the *MOSFLM* (Leslie, 1992) package and scaled using *SCALA* (Collaborative Computational Project, Number 4, 1994).

3. Results and discussion

Crystals of the 10 kDa C-terminal subdomain of *C. elegans* Hsp70 were produced that diffract X-rays to ∼3.5 Å for native and ∼4.0 Å for derivative crystals.

3.1. Space-group determination

ceHsp70-CT crystals flash-cooled directly from mother liquor (62% saturated ammonium sulfate, 100 m*M* sodium citrate pH 6.0) diffracted X-rays to approximately 4 Å. Prominent hexagonal ice diffraction rings at ∼3.9, ∼3.62 and ∼3.45 Å were present but did not interfere with data processing (Fig. 3*a*). Initial indexing identified the most likely Bravais lattice to be body-centred tetragonal, with unit-cell parameters $a = b = 196.9$, $c = 200.6$ Å. Analysis of unmerged data with the program *POINTLESS* (Evans, 2006) suggested the cubic Laue group $Im\bar{3}m$ or the tetragonal Laue group $I4/mmm$ as possibilities. Inspection of the systematic absences revealed $(h00) = 2n$, $(0k0) = 2n$ and $(00l) = 4n$ (Fig. 3*c*), consistent with tetragonal space group $I4_122$. Data were successfully indexed and processed to an R_{sym} of ∼10% for native and derivative crystals flash-cooled without cryoprotectant. Unit-cell parameters and data-reduction statistics are shown in Table 1.

In an effort to improve the diffraction quality of the crystals, a series of cryoprotectants were screened. Of these, crystals vitrified in 70% ammonium sulfate, 10% glycerol and 100 m*M* sodium citrate pH 6.0 diffracted X-rays to ∼3.4 Å and showed no ice rings (Fig. 3*b*). However, whilst these crystals could be indexed in a tetragonal

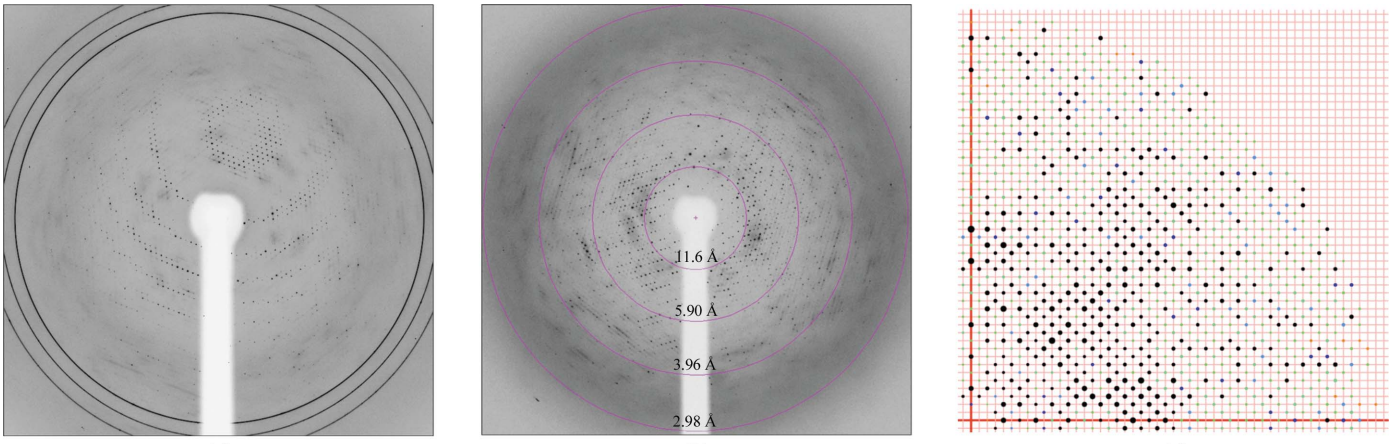

(*a*) (*b*) (*c*)

Figure 3
Diffraction patterns for ceHsp70-CT crystals. (*a*) Native crystal flash-cooled directly from mother liquor (crystal native I). Hexagonal ice diffraction rings are present at ∼3.9, ∼3.62 and ∼3.44 Å. (*b*) Native crystal flash-cooled using 70% saturated ammonium sulfate, 10% glycerol as cryoprotectant (crystal native II). (*c*) Pseudo-precision image showing a section of the 0*kl* zone for native form I data processed in space group $I2_12_12_1$. Reflections show $(0k0) = 2n$ (*x* axis) and $(00l) = 4n$ (*y* axis). Produced with *XPREP* (Bruker AXS, Madison, USA).

Table 2
Anomalous signal statistics for the mercury-derivative data processed in space groups $I4_122$ and $I2_12_12_1$.

A signal-to-noise ratio greater than 1.2 indicates significant anomalous signal, where 0.8 indicates noise. Data were truncated where the correlation coefficient between the signed anomalous differences was greater than ∼30%.

Resolution (Å)	∞–8.0	8.0–6.0	6.0–5.6	5.6–5.4	5.4–5.2	5.2–5.0	5.0–4.8	4.8–4.6	4.6–4.4	4.4–4.2	4.2–3.95
Statistics of the anomalous signal-to-noise ratio against resolution, $\langle\lvert F^+ - F^-\rvert/\sigma(F^+ - F^-)\rangle$											
$I4_122$											
Peak	2.93	1.87	1.39	1.17	1.12	1.07	0.98	0.95	0.84	0.81	0.78
Inflection	1.82	1.06	0.90	0.91	0.83	0.75	0.78	0.74	0.80	0.83	0.79
$I2_12_12_1$											
Peak	2.26	1.52	1.17	1.01	1.02	0.94	0.89	0.85	0.80	0.74	0.74
Inflection	1.46	0.95	0.84	0.78	0.72	0.75	0.77	0.79	0.83	0.75	0.739
Correlation coefficient between the signed anomalous differences against resolution, CC $[(F^+ - F^-)_i, (F^+ - F^-)_j]$											
$I4_122$											
Peak/inflection	84.5	55.8	39.0	30.7	16.0	23.9	18.2	3.5	−0.3	11.1	16.5
$I2_12_12_1$											
Peak/inflection	58.9	43.7	29.0	20.1	8.3	12.8	16.0	7.3	−0.4	5.8	10.6

lattice, the merging statistics were poor (R_{sym} = 29.1% for data processed in $I4_122$). Reprocessing in the orthorhombic space group $I222$ (or $I2_12_12_1$) resulted in an improved R_{sym} of 15.5%, albeit still high (Table 1, native II). $I4_122$ constitutes a minimal non-isomorphic supergroup of space group $I2_12_12_1$ (Hahn, 2002) and data have been processed in both tetragonal and orthorhombic space groups for comparison (Table 1). The possibility of twinning was investigated, but no indication was present in the cumulative intensity distribution or in the plots of accentric and centric moments of E as output by the program *TRUNCATE* (French & Wilson, 1978).

3.2. Content of the asymmetric unit

For a protein with molecular weight 13 094 Da, the Matthews equation (Matthews, 1968) indicates there to be between nine (V_M = 4.09 Å^3 Da^{-1}, solvent content = 70%) and 21 monomers (V_M = 1.75 Å^3 Da^{-1}, solvent content = 30%) per asymmetric unit for packing in $I4_122$ and between 18 and 42 for space group $I2_12_12_1$. Hsp70 has been shown to form dimers, trimers and higher order oligomers in solution (Benaroudj *et al.*, 1995, 1996, 1997; Fouchaq *et al.*, 1999; Chou *et al.*, 2003; Nemoto *et al.*, 2006) and a related domain from rat crystallized with four monomers in the asymmetric unit as two dimers in a cruciform-like arrangement (Chou *et al.*, 2003). However, gel-filtration studies demonstrated that ceHsp70-CT migrated as a single peak with identical retention volume over a wide range of concentrations tested, from less than 0.1 μ*M* to greater than 1 m*M* (data not shown). Glutaraldehyde cross-linking prior to gel filtration revealed this peak to be consistent with the monomeric species (data not shown).

A self-rotation Patterson map calculated using data processed in space group $I2_12_12_1$ reveals a high degree of rotational non-crystallographic symmetry (Fig. 4). Three orthogonal fourfold axes are present parallel to the crystallographic twofold axes at $\kappa = 90^\circ$. Four mutually orthogonal threefold axes are present aligned parallel to the cell body diagonals at $\kappa = 120^\circ$. Additionally, there are twofold peaks at $\kappa = 180^\circ$ every 45° in the *ab* plane and every 90° parallel to the *ac* and *bc* plane face diagonals. All peaks are approximately the height of the origin and show 432 point-group symmetry, suggesting a pseudo-cubic packing symmetry. Inspection of the native Patterson map also indicates the presence of translational non-crystallographic symmetry, with three large non-origin peaks approximately 20% the height of the origin observed for crystals of space group $I2_12_12_1$ (Fig. 5). This is consistent with the presence of a dimer of trimers or a trimer of dimers related by translational non-crystallographic symmetry at four positions, resulting in 24 monomers in the asymmetric unit and a solvent content of ∼60% (V_M = 3.03 Å^3 Da^{-1}).

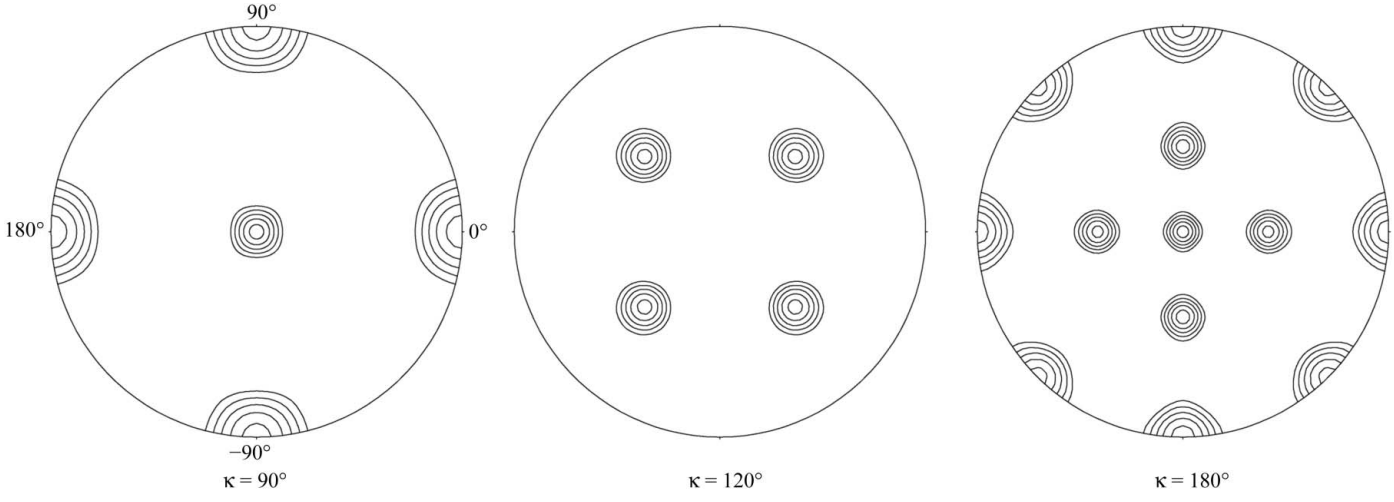

Figure 4
Stereographic projection plots of the κ = 90, 120 and 180° sections of the self-rotation function of the native form II data set. Calculated from data in the resolution range 35–4.0 Å, integration radius 20 Å, showing peaks >30% origin, contour steps at 15%. The data were reduced in $I2_12_12_1$, but the plot shows 432 symmetry. The ω rotation angle is along the radial axis ($\omega = 0^\circ$ in the middle, $\omega = 90^\circ$ on the perimeter) and the φ rotation angle around the perimeter. This figure was prepared with the programs *POLARRFN* and *XPLOT84DRIVER* (Collaborative Computational Project, Number 4, 1994).

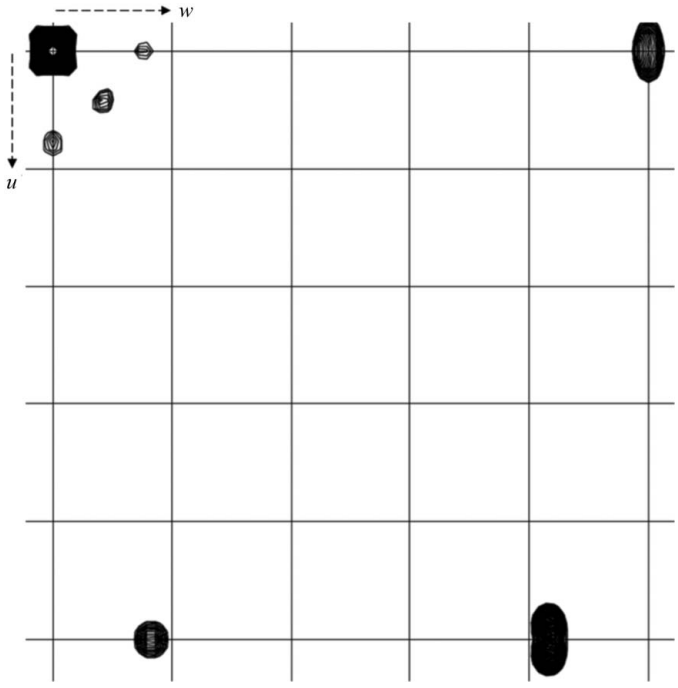

Figure 5
Native Patterson map ($0 < u < 0.5$, $v = 0$, $0 < w < 0.5$) calculated from the native data processed in space group $I2_12_12_1$ using reflections in the resolution range 40–4 Å with $F_{obs} \geq 3\sigma(F_{obs})$. Three large non-origin peaks are observed at (0.4864, 0.0000, 0.4154), (0.5000, 0.0193, 0.0847) and (0.0142, 0.0200, 0.5000) approximately 20% the height of the origin. For data processed in $I4_122$, peaks (0.4864, 0.0000, 0.4154) and (0.5000, 0.0193, 0.0847) are symmetry-related. This figure was prepared with the programs *NPO* and *XPLOT84DRIVER* (Collaborative Computational Project, Number 4, 1994).

3.3. Analysis of MAD data and preliminary phasing

Extensive molecular-replacement trials with both the rat and *E. coli* structures failed to yield a satisfactory solution and were likely to have been complicated by a low signal-to-noise ratio and the presence of translational NCS. For these reasons, a mercury derivative was produced that diffracted X-rays to ∼4 Å, with slightly altered unit-cell parameters along all three axes (Table 1). MAD data were collected at two wavelengths from the same crystal, corresponding to the mercury L_{III} peak (1.005 Å) and inflection point (1.009 Å). Analysis for significant anomalous signal and heavy-atom location was performed with *SHELXC* (Sheldrick, 2004) and *SHELXD* (Schneider & Sheldrick, 2002). An anomalous signal-to-noise ratio based on the mean value of the ratio between the anomalous differences $|F^+ - F^-|$ and the estimated standard deviation of these differences of greater than 1.2 was deemed significant (Sheldrick, 2004). The peak/inflection-point data sets processed in space groups $I4_122$ and $I2_12_12_1$ were estimated to have anomalous signal to 5.4/6.5 Å and 5.6/7 Å respectively (Table 2). The maximum resolution to be included for heavy-atom location, based on a correlation coefficient between the signed anomalous differences ΔF of greater than 30% (Sheldrick, 2004), was estimated to be 5.4 Å ($I4_122$) and 5.6 Å ($I2_12_12_1$) (Table 2). Hsp70-CT contains one cysteine, thus 12 Hg atoms were predicted to be bound in the asymmetric unit for data processed in $I4_122$ and 24 for data processed in $I2_12_12_1$.

For data processed in $I4_122$, *SHELXD* found three strong heavy-atom positions and an additional ten weaker positions, with a sharp drop-off in occupancy between the third and fourth sites (68 and 34%). The heavy-atom substructure was passed to *SHARP* (de La Fortelle & Bricogne, 1997) for maximum-likelihood heavy-atom parameter refinement followed by density modification with

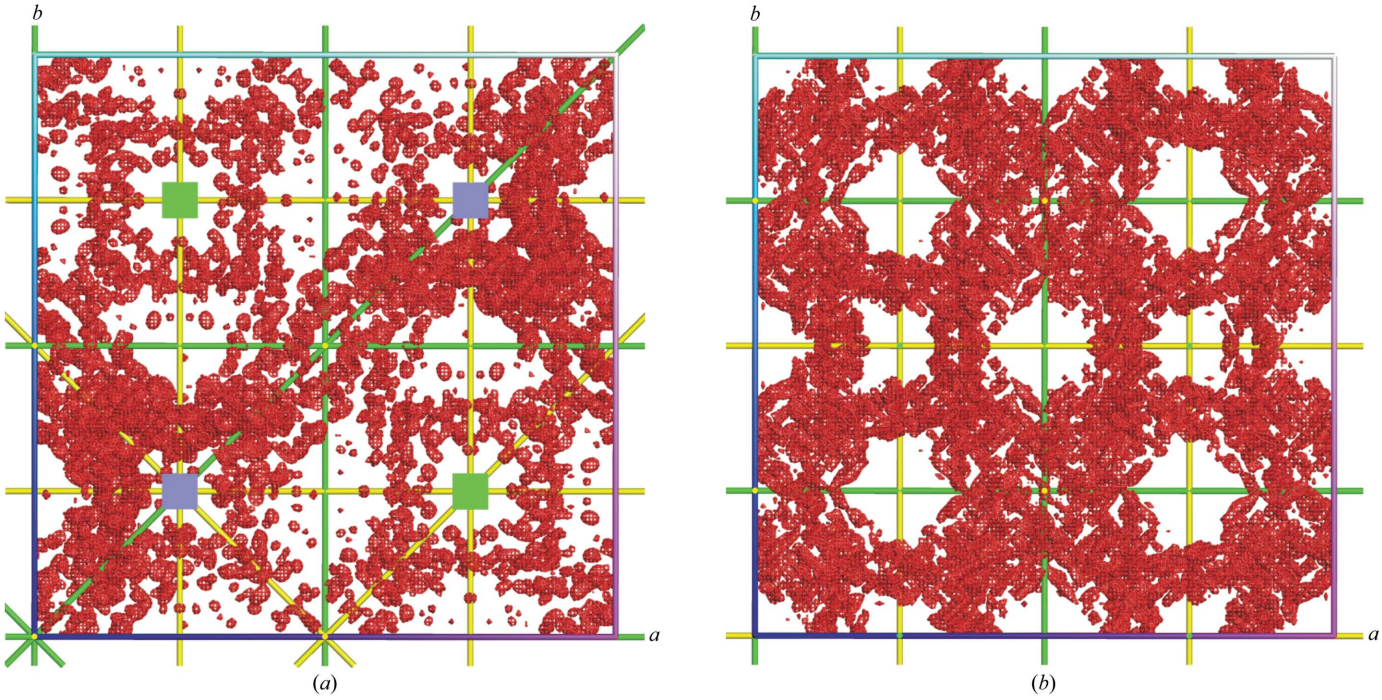

Figure 6
Experimental electron-density maps after phasing and density-modification with *SHARP* and *SOLOMON*, viewed down the unit-cell *c* axis. (*a*) Electron density for data processed in $I4_122$. Interpretable electron density only accounts for 10% of the unit cell, with disordered density evident related by translations consistent with the native Patterson analysis. (*b*) Electron density for data processed in $I2_12_12_1$. Density accounts for all predicted 24 monomers in the asymmetric unit. The unit cellis translated one quarter along the *b* axis compared with (*a*). Twofold axes are shown in yellow and 2_1 screw axes in green; 4_1 screw axes are indicated by green squares and 4_3 screw axes by blue squares. This figure was produced with *PyMOL* (DeLano, 2002).

SOLOMON (Abrahams & Leslie, 1996) using a solvent content of 60%, resulting in a final correlation coefficient on $|E^2|$ of 0.623. The resulting map, whilst noisy, had readily interpretable regions of α-helical secondary structure encompassing the top three heavy-atom positions, with the remaining predicted heavy-atom sites located in areas of disordered density. Despite the interpretable maps, the solution was not in agreement with the analysis of the data. Only three monomers in the asymmetric unit would mean a Matthews coefficient of 12.28 Å^3 Da^{-1} and a predicted solvent content of 90%. In addition, whilst the solution was consistent with the self-rotation function (Fig. 4), the large non-origin Patterson peaks were not (Fig. 5). Regions of disordered density were observable in areas consistent with the native Patterson vectors (Fig. 6*a*), but attempts to locate further heavy atoms failed.

Repeating the procedure with data processed in space group $I2_12_12_1$, *SHELXD* located 27 heavy-atom positions with occupancies ranging from 100 to 13%, with 15 of the sites greater than 50% and no clear drop-off in occupancy. Heavy-atom substructure refinement with *SHARP* resulted in three sites being discarded and density modification with *SOLOMON* led to a map with a final correlation coefficient on $|E^2|$ of 0.684. The resulting map had a clear protein–solvent boundary, with the disordered regions from the $I4_122$ solution now interpretable and all 24 heavy atoms located in regions of protein density (Fig. 6*b*). The crystal lattice is made up of four identical sublattices related by the noncrystallographic translations defined by the native Patterson analysis (Fig. 5).

Further density modification, taking advantage of the high degree of NCS, model building and refinement are currently under way. Use of the derivative phases with the native form II data will allow refinement to 3.4 Å resolution.

We would like to thank Dr Anthony Page, University of Glasgow, for providing the *C. elegans* cDNA. We would also like to thank the beamline scientists at BM14, ESRF, Grenoble for assistance with collection of the MAD data sets. This work was funded by an MRC studentship to LW, a Wellcome Trust grant for EPIC facilities and a BM14 grant.

References

Abrahams, J. P. & Leslie, A. G. W. (1996). *Acta Cryst.* D**52**, 30–42.
Benaroudj, N., Batelier, G., Triniolles, F. & Ladjimi, M. M. (1995). *Biochemistry*, **34**, 15282–15290.
Benaroudj, N., Fouchaq, B. & Ladjimi, M. M. (1997). *J. Biol. Chem.* **272**, 8744–8751.
Benaroudj, N., Triniolles, F. & Ladjimi, M. M. (1996). *J. Biol. Chem.* **271**, 18471–18476.
Chappell, T. G., Konforti, B. B., Schmid, S. L. & Rothman, J. E. (1987). *J. Biol. Chem.* **262**, 746–751.
Chou, C. C., Forouhar, F., Yeh, Y. H., Shr, H. L., Wang, C. & Hsiao, C. D. (2003). *J. Biol. Chem.* **278**, 30311–30316.
Chou, C. C., Wang, C., Sun, Y. J., Shr, H. L. & Hsiao, C. D. (2001). *Acta Cryst.* D**57**, 1928–1930.
Collaborative Computational Project, Number 4 (1994). *Acta Cryst.* D**50**, 760–763.
DeLano, W. L. (2002). *The PyMOL Molecular Visualization System*. http://www.pymol.org.
Diederichs, K. & Karplus, P. A. (1997). *Nature Struct. Biol.* **4**, 269–275.
Edgar, R. C. (2004). *Nucleic Acids Res.* **32**, 1792–1797.
Evans, P. (2006). *Acta Cryst.* D**62**, 72–82.
Fernandez-Saiz, V., Moro, F., Arismendi, J. M., Acebron, S. P. & Muga, A. (2006). *J. Biol. Chem.* **281**, 7479–7488.
Flaherty, K. M., DeLuca-Flaherty, C. & McKay, D. B. (1990). *Nature (London)*, **346**, 623–628.
Flynn, G. C., Chappell, T. G. & Rothman, J. E. (1989). *Science*, **245**, 385–390.
Fouchaq, B., Benaroudj, N., Ebel, C. & Ladjimi, M. M. (1999). *Eur. J. Biochem.* **259**, 379–384.
French, S. & Wilson, K. (1978). *Acta Cryst.* A**34**, 517–525.
Hahn, T. (2002). *International Tables for Crystallography*, Vol. *A*, 5th ed. Dordrecht: Kluwer Academic Publishers.
Jiang, J., Prasad, K., Lafer, E. M. & Sousa, R. (2005). *Mol. Cell*, **20**, 513–524.
La Fortelle, E. de & Bricogne, G. (1997). *Methods Enzymol.* **276**, 472–494.
Leslie, A. G. W. (1992). *Jnt CCP4/ESF–EACBM Newsl. Protein Crystallogr.* **26**.
Matthews, B. W. (1968). *J. Mol. Biol.* **33**, 491–497.
Mayer, M. P., Schroder, H., Rudiger, S., Paal, K., Laufen, T. & Bukau, B. (2000). *Nature Struct. Biol.* **7**, 586–593.
Morshauser, R. C., Hu, W., Wang, H., Pang, Y., Flynn, G. C. & Zuiderweg, E. R. (1999). *J. Mol. Biol.* **289**, 1387–1403.
Nemoto, T. K., Fukuma, Y., Itoh, H., Takagi, T. & Ono, T. (2006). *J. Biochem. (Tokyo)*, **139**, 677–687.
Pellecchia, M., Montgomery, D. L., Stevens, S. Y., Vander Kooi, C. W., Feng, H. P., Gierasch, L. M. & Zuiderweg, E. R. (2000). *Nature Struct. Biol.* **7**, 298–303.
Rist, W., Graf, C., Bukau, B. & Mayer, M. P. (2006). *J. Biol. Chem.* **281**, 16493–16501.
Schneider, T. R. & Sheldrick, G. M. (2002). *Acta Cryst.* D**58**, 1772–1779.
Sheldrick, G. M. (2004). *SHELX*. http://shelx.uni-ac.gwdg.de/SHELX/.
Takeda, S. & McKay, D. B. (1996). *Biochemistry*, **35**, 4636–4644.
Wang, H., Kurochkin, A. V., Pang, Y., Hu, W., Flynn, G. C. & Zuiderweg, E. R. (1998). *Biochemistry*, **37**, 7929–7940.
Wegele, H., Muller, L. & Buchner, J. (2004). *Rev. Physiol. Biochem. Pharmacol.* **151**, 1–44.
Zhu, X., Zhao, X., Burkholder, W. F., Gragerov, A., Ogata, C. M., Gottesman, M. E. & Hendrickson, W. A. (1996). *Science*, **272**, 1606–1614.